ACTIVE AND REACTIVE POWER CONTROL IN A THREE-PHASE GRID-CONNECTED PV POWER SYSTEM USING DQ0 TRANSFORMATION

Mateus F. Schonardie, Roberto F. Coelho, Lenon Schmitz, Denizar C. Martins.
Federal University of Santa Catarina
Department of Electrical Engineering – Power Electronics Institute
P. O. Box 5119, Zip Code: 88040-970 – Florianopolis, SC – Brazil
denizar@inep.ufsc.br

***Abstract* – This work proposes a 12 kW three-phase grid-connected single stage PWM DC-AC converter destined to process the energy provided by a photovoltaic array composed of 57 KC200GT PV modules with high power factor for any solar radiation. The PWM inverter modeling and the control strategy, using *dq0* transformation, are proposed in order to also allow the system operation as an active power filter, capable to compensate harmonic components and reactive power generated by the non-linear loads connected to the mains grid. An input voltage clamping technique is proposed to impose the photovoltaic operation on the maximum power point. Simulation and experimental results are presented to validate the proposed methodology for grid connected photovoltaic generation system.**

***Keywords* – Grid-Connected PV Systems, *dq0* Transformation, Active and Reactive Power, Three-Phase DC-AC PWM Converter.**

I. INTRODUCTION

For decades the electrical energy matrix was based almost exclusively on non-renewable sources: oil, gas, coal and nuclear power plant. The energy crisis, in 1973, associated to the government incentive and cost reduction, allowed the gradual employment of Renewable Energy Sources (RES) as a non-pollutant and alternative sources of electrical energy.

Firstly, photovoltaic (PV) systems were widely used to provide energy to remote areas, in standalone applications. However, with the power electronic development and the possibility to connected photovoltaic systems to the mains, resulting in the grid-connected photovoltaic systems.

Commonly, the grid-connection is achieved by the employment of power converters, capable to process the photovoltaic generated energy and to provide it to the grid, ensuring high power factor and the grid current quality. In this context, several papers have been published, concerning the study of topologies and control strategies for three-phase converters applied to grid-connection [1 - 9].

This paper proposes a 12 kW three-phase grid-connected single stage PWM DC-AC converter destined to process the energy provided by a photovoltaic array composed of 57 KC200GT photovoltaic modules (Figure 1). The main features associated to the proposed system are:

- Capability to supply any AC loads, including the non-linear ones;
- Provident of active power to the main grid;
- Active power filter function - compensation of instantaneous reactive power caused by non-linear loads connected to the system [10];
- Operation near unity power factor for any solar radiation;
- UPS function for any kind of load;
- Energy flow control between the photovoltaic array and the grid;
- Maximum power point tracking accomplishment, ensuring the photovoltaic array operation on the optimal point.

In order to reach all these purposes, a complete system analysis is presented, including the converter mathematical modeling using *dq0* transformation, a control strategy for grid current and dc bus voltage compensation and both, simulation and experimental results, validating the system theoretical study.

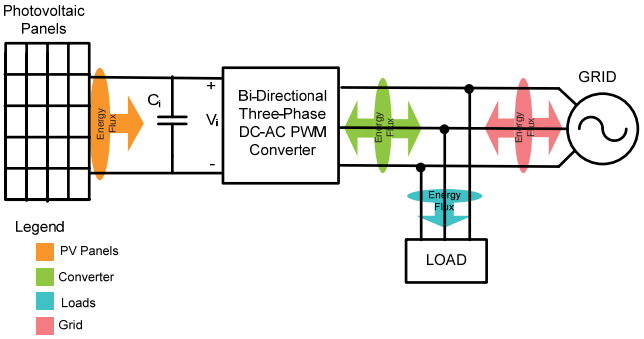

Fig. 1. Proposed three-phase photovoltaic power system.

II. PHOTOVOLTAIC ARRAY DESIGN

A photovoltaic array is an interconnection of modules made up of many PV cells in parallel or series to obtain the desired power. In this paper a PV array using Kyocera KC200 was designed to validate the proposed methodology. The Kyocera KC200 module specifications are showing in Table I.

TABLE I
Kyocera KC200 Electrical Specifications.

Maximum Power	200 W
Maximum Power Voltage	26.3 V
Maximum Power Current	7.61 A
Open Circuit Voltage	32.9 V
Short Circuit Current	8.21 A

The array was connected in a proper series-parallel configuration as shown in Figure 2. Table II shows the main characteristics of the PV array, which was designed to close

Manuscript received 11/12/2012. First revision on 19/04/2013, second revision on 04/08/2013. Accepted for publication in 04/08/2013, by recommendation of the Editor Henrique A. C. Braga.

near 500 Volts photovoltaic output voltage and power of 11.4 kilowatts. To simulate the PV array, it was used the equivalent circuit shown in Figure 3.

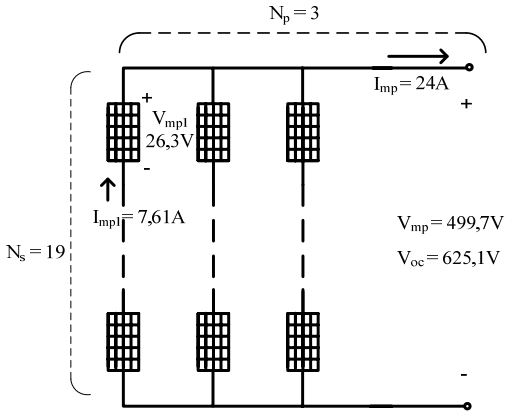

Fig. 2. PV Array designed.

TABLE II
PV array Specifications using Kyocera KC200 panels.

Total peak Power	11.4 kW
Number of series modules (strings) – Ns	19
Number of paralel strings – Np	3
Number of PV modules	57
Maximum Power Current	22.8 A
Maximum Power Voltage	499.7 V
Current: short circuit	24.6 A
Voltage: open circuit	625.1 V

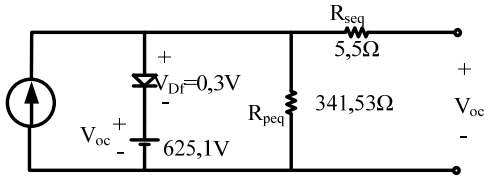

Fig. 3. PV Array simulated circuit.

In the proposed photovoltaic array modeling, the DC voltage source represents the open circuit voltage of all series photovoltaic modules, while the diode imposes its semiconductor characteristic.

III. MODELING OF THE CONVERTER

The converter modeling is relatively simple and it is accomplished through *dq0* transformation. To apply the proposed methodology it is necessary to obtain the voltage and current modeling.

A. The three-phase converter

The converter proposed in this work is a three-phase bi-directional DC-AC converter with PWM modulation using six power switches. The simplified electrical diagram of the converter is shown in Figure 4.

The bi-directional characteristic of the converter is very important in this proposed photovoltaic system, because it allows the processing of active and reactive power from the generator to the load and vice-versa, depending on the application. Thus, with an appropriate control of the power switches it is possible to control the active and reactive power flow.

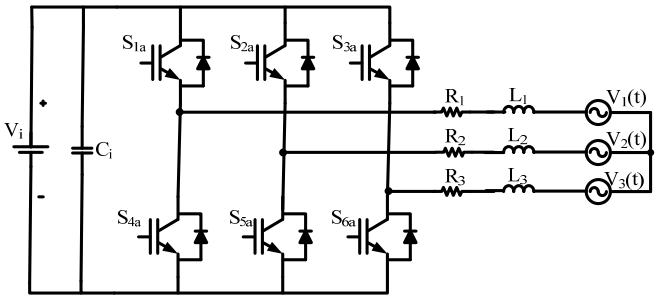

Fig. 4. Bi-directional DC-AC PWM converter.

B. Voltage Control Modelling

The purpose of this modeling is to accomplish the active input voltage clamping $V_i(t)$. This active clamping brings the following advantages:

- Control of the power flow between grid and PV system;
- Possibility to realize the Maximum Power Point Tracking (MPPT) of the PV panels.

The possibility of MPP operation is based on the constant voltage method that is achieved by keeping the voltage in the PV terminals constant and close to the MPP [11], [12]. In Figure 5 an example of the current and voltage characteristics of a PV cell for different values of solar irradiation is presented.

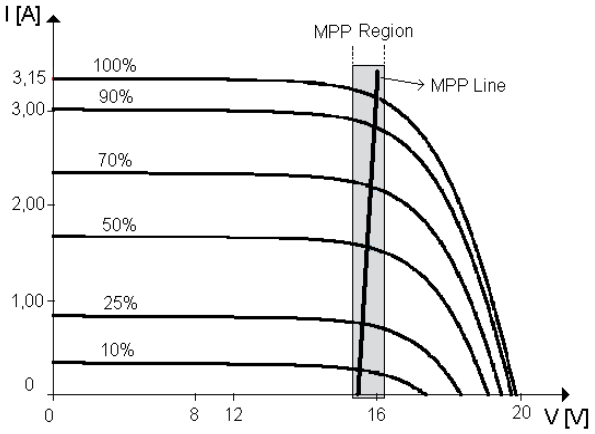

Fig. 5. Example of the current and voltage characteristics of a PV cell.

Observing the MPP points (MPP Line), it is possible to notice that the voltage values vary very little even when the intensity of the solar irradiation suffers great alterations. Concern to the temperature, fortunately, the region in Brazil, which this system is implemented, the temperature has no important variation during the day. So, the experimental tests show that this MPP technique can be used, in this case, without any problem.

With the voltage clamped in a value "inside" of the *MPP Region*, when a variation of the solar irradiation happens, the intensity of the PV cell current also changes; however, the output voltage of the PV cell will not be altered drastically.

Thus, it is necessary to obtain the transfer function of the input voltage V_i as functions of the axis *d* and *q* currents.

The control voltage across capacitor C_i is obtained considering the DC input voltage shown in Figure 4. The equivalent circuit in *dq0* axis, seen by the DC side, is shown in Figure 6.

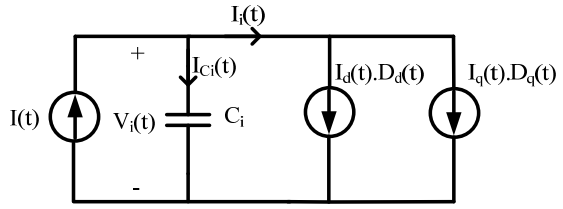

Fig. 6. Equivalent circuit seen by the DC side.

In this equivalent circuit, I(t) represents the current supplied by PV panels (1) and $I_i(t)$ represents the input inverter current (2). The transfer function between voltage $v_i(s)$ and input current of the inverter $i_i(s)$ is shown in (3).

$$I(t) = I_{Ci}(t) + I_i(t) \tag{1}$$

$$I_i(t) = I_d(t) \cdot D_d(t) + I_q(t) \cdot D_q(t) \tag{2}$$

$$\frac{v_i(s)}{i_{Ci}(s)} = -\frac{1}{s \cdot C_i} \tag{3}$$

Developing and substituting appropriately the equations, it is possible to obtain the desired voltage control modeling. The equations $v_i(s)$ as function of the currents in axis *d* and *q* are shown in (4) and (5), respectively.

$$\frac{v_i(s)}{i_d(s)} = \frac{1}{s \cdot C_i} \cdot \left[\left(-K \cdot L \cdot s\right) - 2 \cdot K \cdot R + \frac{\sqrt{3}}{\sqrt{2}} \cdot \frac{V_p}{V_i} \right] \tag{4}$$

$$\frac{v_i(s)}{i_q(s)} = -\frac{\sqrt{2}}{\sqrt{3}} \cdot \frac{Q}{V_i \cdot V_p} \cdot \left[\frac{L \cdot s + 2 \cdot R}{s \cdot C_i} \right] \tag{5}$$

where:

L, R - Equivalent resistances and inductances;

C_i - Input capacitor;

V_p - Voltage peak of the grid;

V_i - Input voltage;

i_d, i_q - Currents in the axis *d* and *q*, respectively;

P - Active power;

Q - Reactive power;

$$K = \frac{\sqrt{2}}{\sqrt{3}} \frac{P}{V_p \cdot V_i}.$$

C. Current Control Modeling

The modeling for the current control is obtained considering the AC output. When the circuit is observed from the AC output, it is possible to make some initial considerations that result in a simplified circuit [13], shown in Figure 7. The line voltages are presented in (6) considering $L_1=L_2=L_3=L$, $R_1=R_2=R_3=R$ and D are the duty cycle.

$$\begin{cases} V_{12}(t) = L \cdot \dfrac{dI_{12}(t)}{dt} + D_{12}(t) \cdot V_i + R \cdot I_{12}(t) \\ V_{23}(t) = L \cdot \dfrac{dI_{23}(t)}{dt} + D_{23}(t) \cdot V_i + R \cdot I_{23}(t) \\ V_{31}(t) = L \cdot \dfrac{dI_{31}(t)}{dt} + D_{31}(t) \cdot V_i + R \cdot I_{31}(t) \end{cases} \tag{6}$$

Applying *dq0* transformation and developing the equations system (6), it is possible to find the differential equations (7), which describe the currents behavior in axis *d* and *q*.

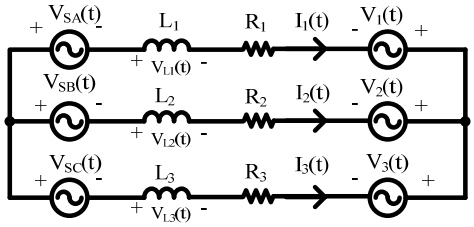

Fig. 7. Simplified circuit from AC output.

$$\begin{cases} \dfrac{dI_d(t)}{dt} = \omega \cdot I_q(t) + \sqrt{\dfrac{3}{2}} \cdot \dfrac{V_p}{L} - \dfrac{V_i}{L} \cdot D_d(t) - \dfrac{R \cdot I_d(t)}{L} \\ \dfrac{dI_q(t)}{dt} = -\omega \cdot I_d(t) - \dfrac{V_i}{L} \cdot D_q(t) - \dfrac{R \cdot I_q(t)}{L} \end{cases} \tag{7}$$

The direct axis current depends on the quadrature axis current and vice-versa. In order to decouple this dependence, a new duty cycle was defined and it is presented in (8).

$$\begin{cases} D'_d(t) = D_d(t) - \dfrac{\omega \cdot L}{V_i} \cdot I_q(t) \\ D'_q(t) = D_q(t) + \dfrac{\omega \cdot L}{V_i} \cdot I_d(t) \end{cases} \tag{8}$$

If $D_d(t)$ and $D_q(t)$ were isolated in (8), it is possible to rewrite (7) as follow:

$$\begin{cases} \dfrac{dI_d(t)}{dt} = \sqrt{\dfrac{3}{2}} \cdot \dfrac{V_p}{L} - \dfrac{V_i}{L} \cdot D'_d(t) - \dfrac{R \cdot I_d(t)}{L} \\ \dfrac{dI_q(t)}{dt} = -\dfrac{V_i}{L} \cdot D'_q(t) - \dfrac{R \cdot I_q(t)}{L} \end{cases} \tag{9}$$

Developing appropriately these equations, it is possible to obtain the differential equations that show the behavior of the currents in axis *d* and *q* as functions of the duty cycles. So, the transfer functions used in the design of the current controllers are shown in (10).

$$\begin{cases} \dfrac{i_d(s)}{d'_d(s)} = -\dfrac{V_i}{s \cdot L + R} \\ \dfrac{i_q(s)}{d'_q(s)} = -\dfrac{V_i}{s \cdot L + R} \end{cases} \tag{10}$$

In this current control modeling, the line duty cycles ($D_{12}(t)$, $D_{23}(t)$, $D_{31}(t)$) are used in all the equations. Nevertheless, to satisfy the PWM modulation, it is necessary to determine the phase duty cycles ($D_1(t)$, $D_2(t)$, $D_3(t)$). This is obtained by Δ/Y transformation shown in (11).

$$\begin{bmatrix} D_1(t) \\ D_2(t) \\ D_3(t) \end{bmatrix} = \begin{bmatrix} 1/3 & 0 & -1/3 \\ -1/3 & 1/3 & 0 \\ 0 & -1/3 & 1/3 \end{bmatrix} \cdot \begin{bmatrix} D_{12}(t) \\ D_{23}(t) \\ D_{31}(t) \end{bmatrix} \tag{11}$$

IV. IMPLEMENTATION OF THE CONTROL METHODOLOGY

Figure 8 shows the diagram of the control methodology and the modulation of the proposed three-phase grid-connected PV system. The practical implementation of control strategy and a zero cross detector circuit to make the synchronism with the grid have been implemented through DSP (Digital Signal Processing) device.

As can be seen from Figure 8, the inverter output currents (I_1, I_2 and I_3) and the load currents (I_{1c}, I_{2c} and I_{3c}) are acquired through sensors. In the line currents it is applied *dq0* transformation.

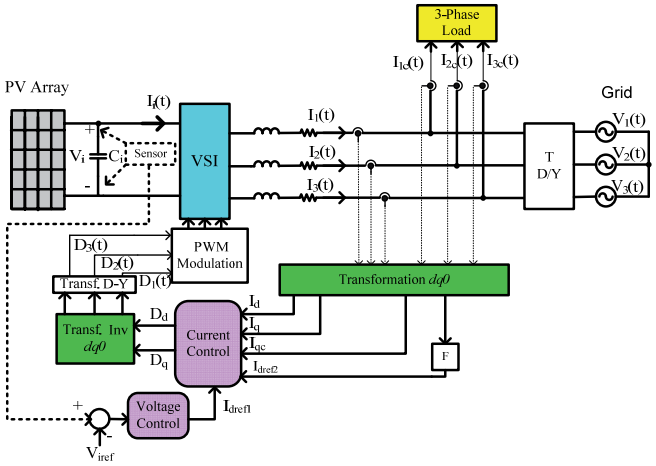

Fig. 8. Diagram of the control system.

A. Current control strategy

To control the currents of the axis *d*, the current $I_d(t)$ and the reference currents $I_{dref1}(t)$ and $I_{dref2}(t)$ are used, according to Figure 9. The sign $I_{dref2}(t)$ represents the alternate portion of the current $I_{dc}(t)$ in the direct axis *d* and it is obtained through a high-pass filter (Figure 10) [14]. This strategy is necessary to compensate possible power unbalances in the system.

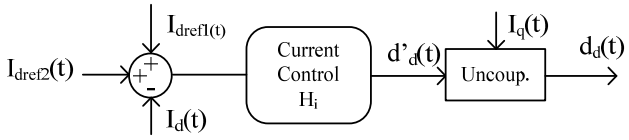

Fig. 9. Block diagram of the current control in the *d* axis.

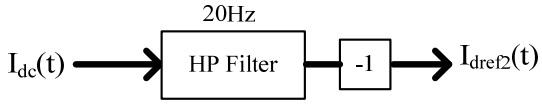

Fig. 10. $I_{dref2}(t)$ obtaining.

To control the currents of axis *q* (Figure 11), a reference signal $I_{qc}(t)$ is used to compensate the reactive power caused by the load connected to the system.

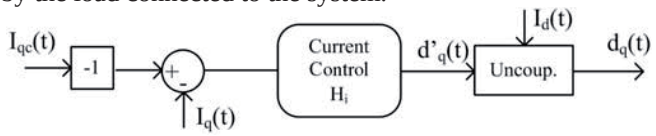

Fig. 11. Block diagram of the current control in the axis *q*.

In the output of both controls (*d* and *q* axis) it is necessary to accomplish an uncoupling in order to obtain the duty cycles $d_d(t)$ as function of $i_d(t)$ and $d_q(t)$ as function of $i_q(t)$.

B. Voltage control strategy

The voltage in the capacitor C_i is compared with the reference voltage V_{iref} and the error signal enters in the voltage controller, resulting in the signal $I_{dref1}(t)$ (Figure 12).

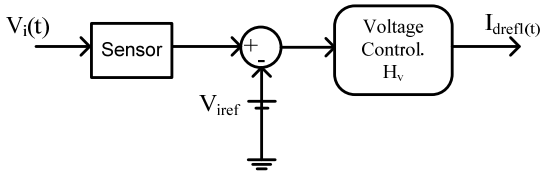

Fig. 12. Diagram of the voltage regulator.

The signal $I_{dref1}(t)$ is used as one of the references in the current control loop of the direct axis *d*, guaranteeing that the voltage $V_i(t)$ keeps clamped at the desired value, as shown in Figure 13.

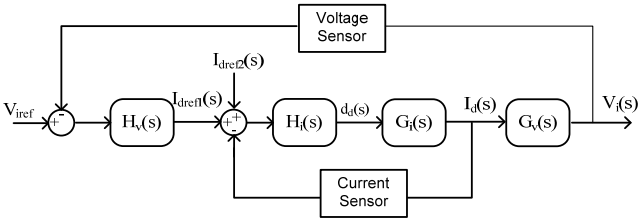

Fig. 13. Block diagram of the voltage control.

V. SIMULATION RESULTS

Numerical simulations were accomplished for different situations of loads and solar radiations. The simulations of the loads connected in the system are linear and non-linear types.

For simulating it was used the parameters of the converter show in Table III. The simulation with linear loads was done and good results were obtained to several load parameters. Figure 14 presents the behavior of current and voltage in phase 1 when the PV array begins sending power to the system. In this figure it is also shown the output currents of the converter and the load. It is possible to see that the PV array is supplying almost the entire current to the load, so the current in the phase 1 of the grid has a small value.

Table III
Converter simulation parameters.

Parameters	Description
P = 11.4 kVA	- Converter Power
Vi= 500 V	- Input Voltage (DC)
Vout= 127 V	- RMS Output Voltage (grid)
fr= 60 Hz	- Grid Frequency
fs = 20 kHz	- Commutation Frequency
R = 0.57 Ω	- Output inverter equivalent resistor
L = 1.92 mH	- Output inverter equivalent inductance
Ci= 4.7 mF	- Input inverter capacitor

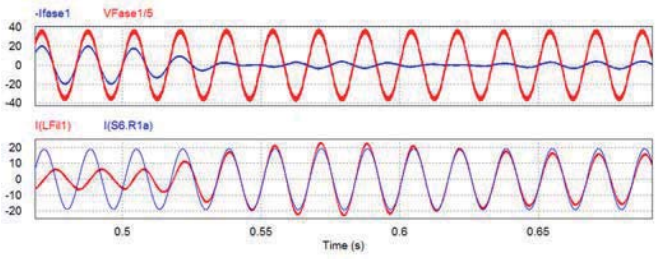

Fig. 14. Linear load simulation: Ipv=10A – Grid voltage and current (phase 1), Load current and output inverter current (phase1).

The same currents shown in Figure 14 are also seen in Figure 15 at the instant where the current of the PV array increases from 10 A to 20 A. The excess of the energy that does not consumed by the load is injected to the grid with high quality, as shown in Figure 15. In this moment, the grid input current waveform is sinusoidal and is 180° out of phase to the grid voltage. In others words, part of the energy from the PV array supplies the RL load and the additional energy is inserted into the grid.

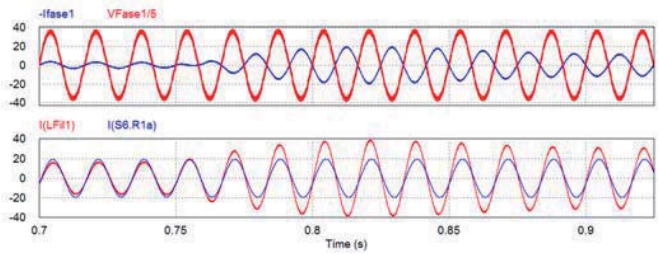

Fig. 15. Linear load simulation: Ipv=20A – Grid voltage and current (phase 1), Load current and output inverter current (phase1).

To show a better performance of the proposed system, the results considering non-linear loads connected to the system are presented. The non-linear load is a three-phase bridge rectifier with RC output, shown in Figure 16. With this kind of load the performance of the reactive power compensation and harmonics current elimination is better observed when tests are done.

The simulation presents the behavior of the system for several situations of abrupt variations of the current supplied by the PV panels. Figure 17 shows in the phase 1 the grid voltage, grid current, load current, output inverter current and input voltage $V_i(t)$ for the moment that the PV current is null. Observing the current and voltage of the grid there is no processing energy from the sun, it is noted that the current is in phase with the voltage. During this period, the converter is operating only to correct the power factor of the system.

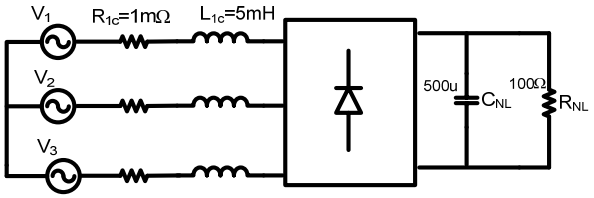

Fig. 16. Non-linear load simulated.

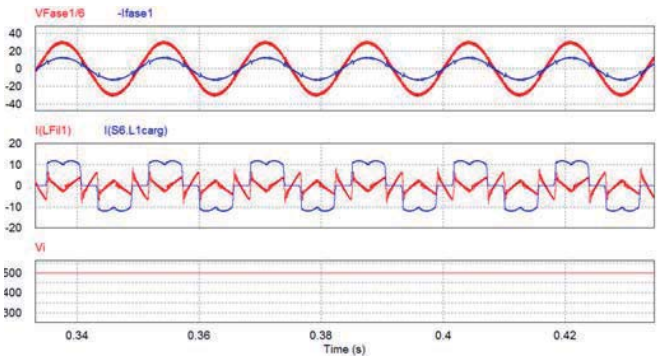

Fig. 17. Grid voltage and current (phase 1), Load current and output inverter current (phase1); and Input voltage.

Figure 18 shows, in the phase 1, the grid voltage, grid current, load current and output inverter current behavior, when a variation of the current supplied by the PV panels occurs at the instant t = 0.75 s. Even with non-linear load, the grid current waveform is sinusoidal and is 180° out of phase to the grid voltage. This situation means that the grid is receiving energy from the PV panels.

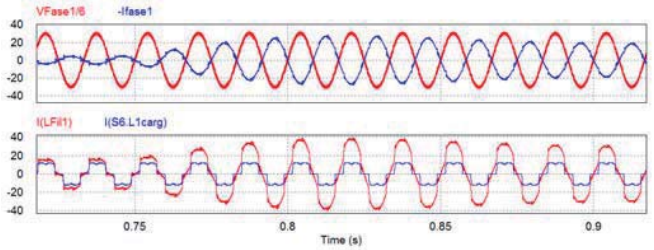

Fig. 18. No-linear load simulation: Grid voltage and current (phase 1), Load current and output inverter current (phase1).

Figure 19 shows the behavior of the current and voltage in phase 1 of the grid, when another abrupt variation of the current supplied by PV panels occurs. In the absence of the PV panel energy, the converter only acts as an active power filter. The inverter output current and the load current are also shown in Figure 19.

Even with this abrupt variation, the voltage control maintains the desired level of the DC Bus (500 V) with high power factor. The input voltage $V_i(t)$ behavior is shown in Figure 20.

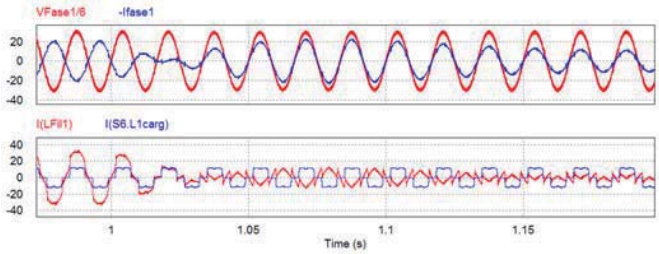

Fig. 19. No-linear load: Grid voltage and current (phase 1), Load current and output inverter current (phase1).

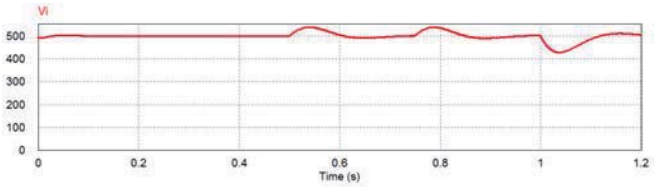

Fig. 20. Behavior of the voltage V_i.

To validate the structure operation as active power filter, Figure 21 shows the grid and load current harmonic spectrum in the phase 1. It has been verified that using the proposed control strategy, it is possible to eliminate the harmonic components of the grid current.

VI. EXPERIMENTAL RESULTS

To demonstrate the feasibility of the discussed PV system, a prototype was designed and implemented following the specifications presented in Tables II and III. Figure 22 depicts in the phase 1 the utility voltage ($V_{Utility}$) and utility

current (I_S) with the system operating just in the active power line conditioning mode (cloudy day or night) using only linear load (I_L). Figure 22 shows that the shift angle between voltage and current is compensated satisfactorily.

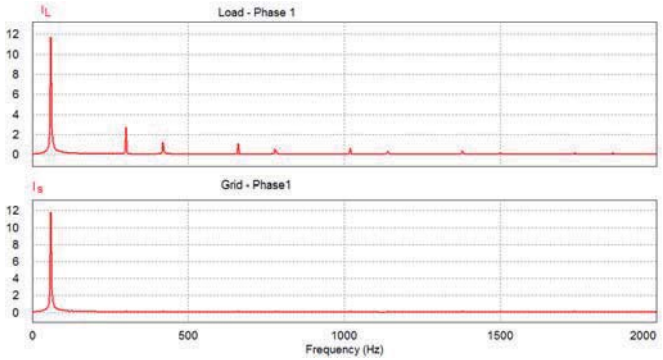

Fig. 21. Current spectrum harmonic.

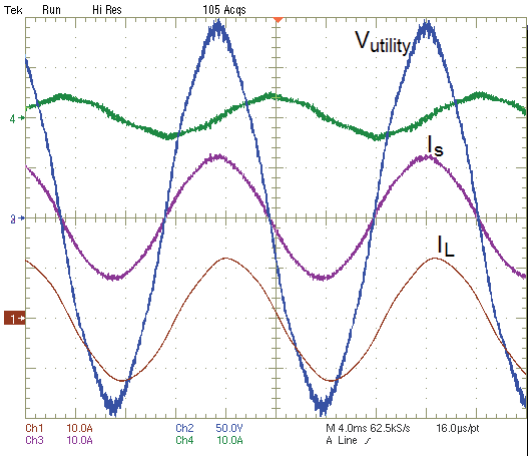

Fig. 22. Operation as Active Filter: utility voltage ($V_{Utility}$), utility current (I_S), load current (I_L), inverter current (green) in phase1 with linear load.

Figure 23 depicts, in the phase 1, the utility voltage ($V_{Utility}$), inverter current ($I_{inverter}$) and utility current (I_S) using non-linear load (I_L). The THD of I_L is 27.5%. The system is also operating just in the active power line conditioning mode.

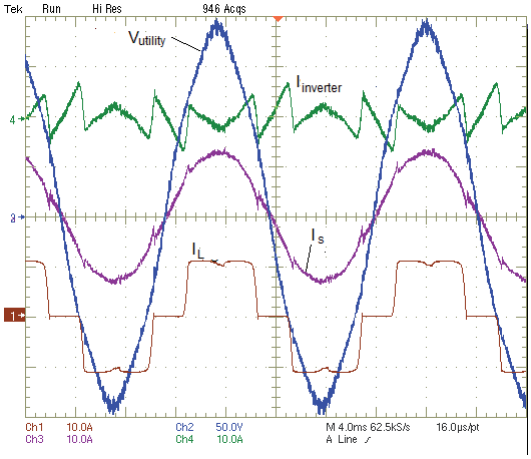

Fig. 23. Operation as Active Filter: utility voltage ($V_{Utility}$), utility current (I_S), load current (I_L), inverter current : phase1 with no-linear load.

Figure 24 shows the utility current harmonic spectrum in the phase 1, where the THD of I_S is 4%. From the presented results it is noted that the proposed system may properly compensate current harmonic components.

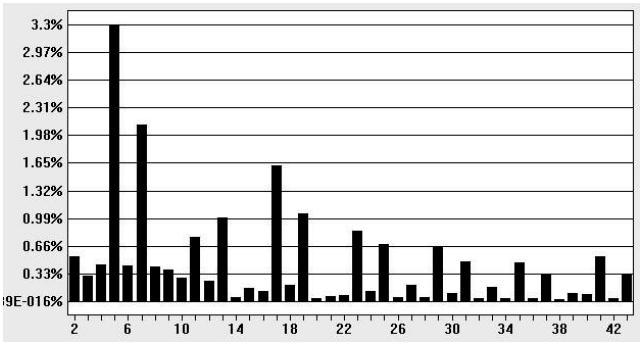

Fig. 24. Utility current harmonic spectrum in the phase 1 for non-linear load.

Figure 25 shows the behavior of the utility voltage ($V_{Utility}$), utility current (I_S) in the phase 1, the load current and the input voltage $V_i(t)$ with non-linear load, which the THD of load current, in this case, is 75% for a crest factor of 3.09. When this non-linear load is employed, the system must operate with highest performance, since it needs to compensate a high harmonic distortion. For this situation, after the system compensation, the THD of the utility current (I_S) is around 5%, as shown in Figure 26.

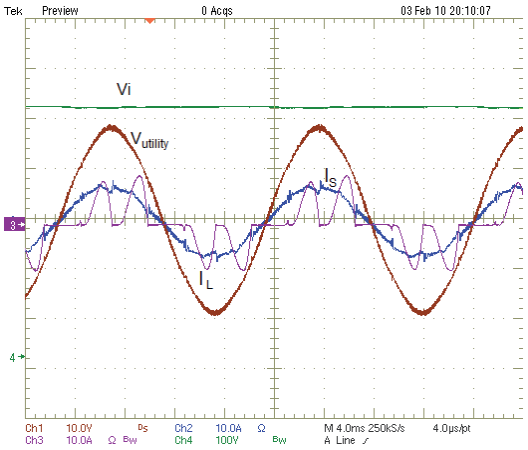

Fig. 25. Operation only as Active Filter: utility voltage ($V_{Utility}$), utility current (I_S), load current (I_L) in phase1: Input voltage (V_i) whit no-linear load.

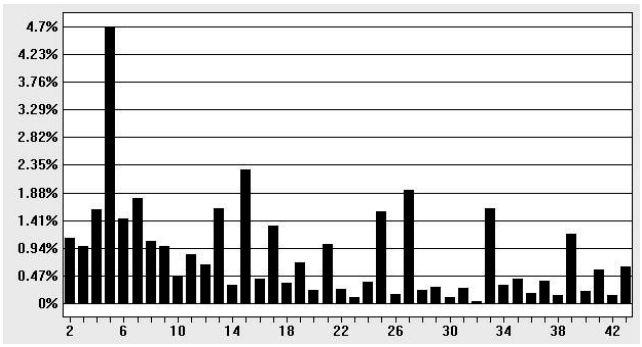

Fig. 26. Utility current harmonic spectrum in the phase 1.

Figure 27 shows the utility voltage and the utility current in the phase 1, with the system only supplying power to the utility grid (THD = 2.5% and PF = 0.998). In this case no load is connected in the PV system. The presented test scenario confirms that the system may control the power flow from the photovoltaic array to the main grid.

Figure 28 presents, for phase 1, with a linear load, the utility voltage ($V_{Utility}$) and utility current (I_S), the current supplied by the PV array (I_{pv}) and the voltage V_i. In this situation, the system operates as an active filter, providing energy to the grid. In addition, it is verified the dc bus voltage Vi remains around the maximum power point voltage, i.e., 463V.

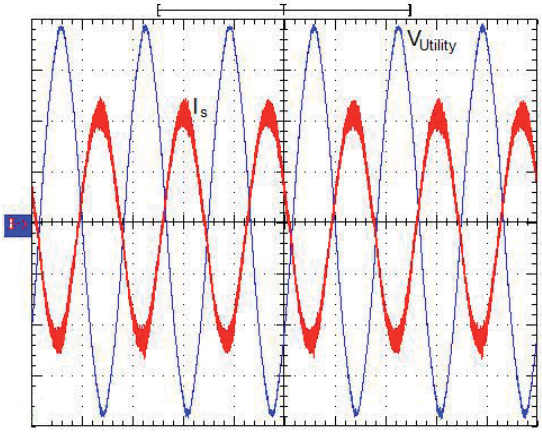

Fig. 27. Utility current (I_S) and utility voltage ($V_{Utility}$) (Ch1 20A/div and Ch2 50V/div).

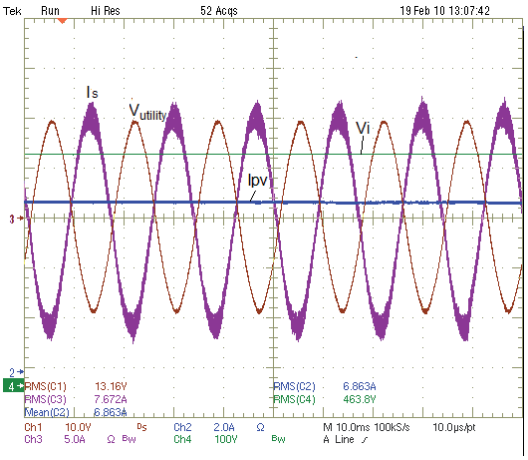

Fig. 28. Utility current (I_S), utility voltage ($V_{Utility}$), PV array curent (I_{pv}) and voltage V_i.

Finally, Figure 29 presents the performance of the utility voltage and utility current (THD = 2.78% and PF = 0.978) for a non-linear load connected between the PV system and the commercial electric grid. The current supplied by the PV array (I_{pv}) is also shown in the Figure. The last test scenario was employed to validate the performance of the system for current harmonic compensating and power flow controlling. Thus, it is possible to employ the proposed structure for processing the PV energy generation, in grid connected applications, as well as, in power factor correction. The efficiency curve of the whole system is shown in Figure 30.

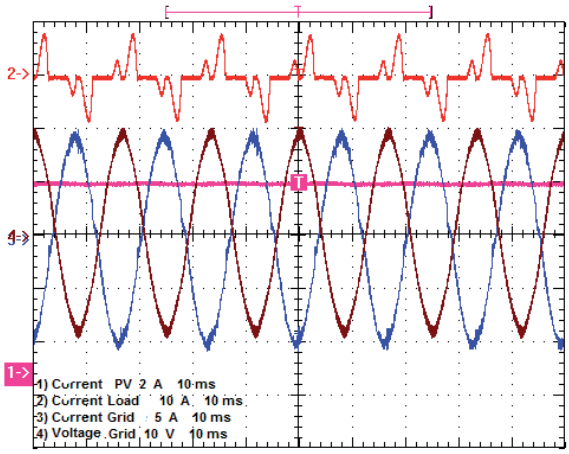

Fig. 29. Utility current, utility voltage, PV array current, and load current.

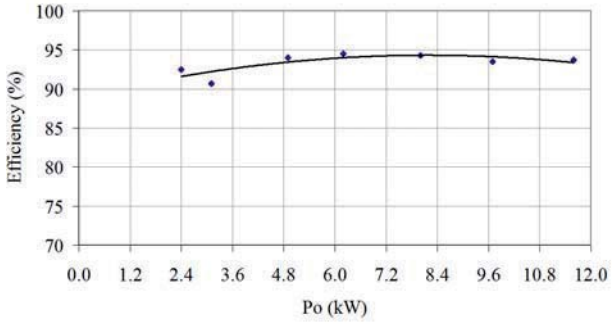

Fig. 30. Efficiency curve of the whole system.

VII. CONCLUSION

Since renewable energy source became a reality, several topologies and control techniques were developed in order to ensure the quality of the grid current, reducing its THD and raising the power factor. This paper has presented, in a simple way, the modeling and control strategy using *dq0* transformation of a three-phase PWM inverter to be employed in a grid-connected photovoltaic generation system. The main focus of this work consists on the design of a dual function system that would provide solar generation and works as an active power filter, compensating unbalances of power and the reactive power generated by others loads connected to the system. These cited features are quite required for the power quality maintenance, since the grid-connected systems are, today, following some new trends come from the smart grid concept.

It is important to emphasize that for any situations the power factor is always high and the currents present low harmonic distortion.

Due to a little variation of the temperature in the region where the PV panels is implemented, an input voltage clamping technique is used to assure the maximum power point (MPP) of the PV panels.

Validating the structure operation some simulation and experimental results were presented and they show the viability of the proposed modeling, as well as the control strategy used for the PV grid-connected systems.

ACKNOWLEDGEMENT

The authors would like to thanks the CNPq and FINEP by the financial support.

REFERENCES

[1] O. Wasynczuk, N. A. Anwah. Modeling and dynamic performance of a self-commutated photovoltaic inverter system. *IEEE Transactions on Energy Conversion*, vol. 4, Issue 3, pp. 322-328, 1989.

[2] W. Bohrer, M. Carpita, T. Ghiara, L. Puglisi. A flexible control strategy to interface solar system with privileged load and utility line. *Electrotechnical Conference Proceedings. Integrating Research, Industry and Education in Energy and Communication Engineering, MELECON '89*, Mediterranean 11-13, pp. 25-30, 1989.

[3] N. Mohan. A novel approach to minimize line-current harmonics in interfacing renewable energy sources with 3-phase utility systems. In: *Applied Power Electronics Conference and Exposition, APEC '92*. Conference Proceedings, Seventh Annual, pp. 852-858, 1992.

[4] S. Nonaka. A novel three-phase sinusoidal PWM voltage source inverter and its application for photovoltaic power generation system. *In: Power Conversion Conference - Nagaoka, Proceedings of the* vol. 2, pp. 755-758, 1997.

[5] I. H. Hwang, K. S. Ahn, H. C. Lim, S. S. Kim. Design, development and performance of a 50kW grid connected PV system with three phase current-controlled inverter. *In: Conference Record of the 28th IEEE Photovoltaic Specialists Conference*, pp. 1664-1667, 2000.

[6] C. Cecati, A. Dell'Aquila, M. Liserre. A novel three-phase single-stage distributed power inverter. *IEEE Transactions on Power Electronics*, vol. 19, Issue 5, pp.1226-1233, 2004.

[7] I. S. Kim. Robust maximum power point tracker using sliding mode controller for three phase grid connected photovoltaic system. *Solar Energy 81*, pp. 405-414, 2007.

[8] Y. Chen, K. Ma Smedley. One-Cycle-Controller Three-Phase Grid-Connected Inverters and Their Parallel Operation. *IEEE Transctions on Industry Applications*, vol. 44, No. 2, pp. 663-671, March/April, 2008.

[9] R. R. Sawant, M. C. Chandorkar. A Multifunctional Four-Leg Grid-Connected Compensator. . *IEEE Transactions on Industry Applications*, vol. 45, No. 1, pp. 249-259, January/February, 2009.

[10] M. C. Cavalcanti, G. M. S. Azevedo, K C. Oliveira, B. A. Amaral, F. A. S. Neves, Z. D. Lins. A grid connected photovoltaic generation system with harmonic and reactive power compensation. *In: 8th Power Electronics Brazilian Conference, COBEP*, Recife, Brazil, pp. 135-140, 2005.

[11] R. Demonti. Photovoltaic panels electric energy management. Ph.D. Thesis, Florianópolis, Brazil – INEP, UFSC. 2003.

[12] M. J. Case, J. J. Schoeman. A mínimum component photovoltaic array maximum power point tracker. In: *European Space Power Conference*, Granz, Austria, pp. 107-110, 1992.

[13] D. Borgonovo. Modelling and control of the three-phase PWM rectifier using park transformation. Master Thesis in Electrical Engineering, Florianópolis, Brazil – INEP, UFSC, 2001.

[14] A. S. Morais, I. Barbi. Power redistributor applied to distribution transformers of the electrical energy. *In: XVI Brazilian Automation Conference, CBA*, Salvador, Brazil, pp. 334-339, 2006.

BIOGRAPHIES

Mateus Felzke Schonardie was born in Ijuí, RS, Brazil, on November 30, 1977. He was graduated in electrical engineering from the Regional University from Northwest of State of Rio Grande do Sul, RS, Brazil, in 2002 and obtained his M.S. and Ph.D degrees, in power electronics, from Federal University of Santa Catarina, Florianópolis, SC, Brazil, in 2005 and 2011, respectively. Currently, he is a Titular Professor of Electrical Engineering at Regional University from Northwest of State of Rio Grande do Sul. His interest research areas include: dc-ac converters, active power filter, grid-connected PV systems and power factor correction.

Roberto Francisco Coelho was born in Florianópolis, SC, Brazil, on August 19, 1982. He was graduated in electrical engineering and obtained his M.S. degree from Federal University of Santa Catarina, Florianópolis, SC, Brazil, in 2006 and 2008, respectively. Currently, he is a Ph.D candidate on Power Electronics Institute of Federal University of Santa Catarina. His interest research areas include dc-ac and dc-dc converters, active power filters, grid-connected power plants, renewable energy processing systems and power factor correction.

Lenon Schmitz was born in Blumenau, SC, Brazil, on March 28, 1990. He is in the last semester to receive the B.S. degree in electrical engineering from Federal University of Santa Catarina, Florianópolis, SC, Brazil, and he has been a scientific initiation scholarship student at the Power Electronics Institute since 2010. He was co-author in two scientific papers in the grid-connected systems areas. His interest research field includes dc-dc and dc-ac converters, grid-connected systems and renewable energy.

Denizar Cruz Martins was born in São Paulo, Brazil, on April 24, 1955. He received the B.S. and M.S. degrees in electrical engineering from Federal University of Santa Catarina, Florianópolis, SC, Brazil, in 1978 and 1981, respectively, and the Ph.D. degree in electrical engineering from the Polytechnic National Institute of Toulouse, Toulouse, France, in 1986. He is currently a Titular Professor in the Department of Electrical Engineering at Federal University of Santa Catarina. . He is a member of the Brazilian Power Electronics Society. His interest research areas include dc-dc and dc-ac converters, high frequency, soft commutation, power factor correction and grid-connected PV systems.